Bioactive Materials 19 (2023) 653–665

Contents lists available at ScienceDirect

Bioactive Materials

journal homepage: www.keaipublishing.com/en/journals/bioactive-materials

Chitosan@Puerarin hydrogel for accelerated wound healing in diabetic subjects by miR-29ab1 mediated inflammatory axis suppression

Xiaoling Zeng [a,1], Baohui Chen [b,c,1], Luping Wang [a], Yingxiao Sun [a], Zhao Jin [a], Xuanyong Liu [b,e,f,**], Liping Ouyang [a,d,***], Yun Liao [a,*]

[a] Department of Pharmacy, Tongren Hospital, Shanghai Jiao Tong University School of Medicine, Shanghai, 200336, China
[b] State Key Laboratory of High Performance Ceramics and Superfine Microstructure, Shanghai Institute of Ceramics, Chinese Academy of Sciences, Shanghai, 200050, China
[c] Center of Materials Science and Optoelectronics Engineering, University of Chinese Academy of Sciences, Beijing, 100049, China
[d] Hongqiao International Institute of Medicine, Shanghai Jiao Tong University School of Medicine, Shanghai, 200336, China
[e] School of Chemistry and Materials Science, Hangzhou Institute for Advanced Study, University of Chinese Academy of Sciences, 1 Sub-lane Xiangshan, Hangzhou, 310024, China
[f] Cixi Center of Biomaterials Surface Engineering, Shanghai Institute of Ceramics, Chinese Academy of Sciences, Ningbo, 315300, China

ARTICLE INFO

Keywords:
Hydrogel
Diabetic skin wound healing
Macrophages
miR-29ab1

ABSTRACT

Wound healing is one of the major global health concerns in patients with diabetes. Overactivation of pro-inflammatory M1 macrophages is associated with delayed wound healing in diabetes. miR-29ab1 plays a critical role in diabetes-related macrophage inflammation. Hence, inhibition of inflammation and regulation of miR-29 expression have been implicated as new points for skin wound healing. In this study, the traditional Chinese medicine, puerarin, was introduced to construct an injectable and self-healing chitosan@puerarin (C@P) hydrogel. The C@P hydrogel promoted diabetic wound healing and accelerated angiogenesis, which were related to the inhibition of the miR-29 mediated inflammation response. Compared to healthy subjects, miR-29a and miR-29b1 were ectopically increased in the skin wound of the diabetic model, accompanied by upregulated M1-polarization, and elevated levels of IL-1β and TNF-α. Further evaluations by miR-29ab1 knockout mice exhibited superior wound healing and attenuated inflammation. The present results suggested that miR-29ab1 is essential for diabetic wound healing by regulating the inflammatory response. Suppression of miR-29ab1 by the C@P hydrogel has the potential for improving medical approaches for wound repair.

1. Introduction

The usual etiological cause of non-healing chronic skin wounds is diabetes mellitus and associated comorbidities [1]. Wound repair is a complex, yet highly programmed process that includes phases involving hemostasis, inflammatory reactions, cell proliferation, and tissue remodeling [2]. However, the process is halted during the inflammatory phase in chronic skin wounds [3–5]. Delayed wound healing is caused by the overactivation of the inflammatory response in diabetes mellitus, along with associated microvascular and macrovascular diseases [6]. Macrophages play a crucial role in the inflammatory response by dynamically altering their phenotypes and functions. M1 macrophages are known to secrete elevated levels of pro-inflammatory cytokines such as tumor necrosis factor-alpha (TNF-α) and interleukin-1-beta (IL-1β) [7]. M2 macrophages produce polyamines to induce vascular endothelial growth factor (VEGF) expression and collagen production [8]. Failure of the macrophage phenotypic switch from M1 to M2 is associated with impaired wound healing in diabetes [9]. Thus, many attempts have focused on strategies associated with the augmentation of M2 macrophage activity, recruitment of more M2 macrophages, or addition

Peer review under responsibility of KeAi Communications Co., Ltd.
* Corresponding author.
** Corresponding author.State Key Laboratory of High Performance Ceramics and Superfine Microstructure, Shanghai Institute of Ceramics, Chinese Academy of Sciences, Shanghai, 200050, China.
*** Corresponding author.Department of Pharmacy, Tongren Hospital, Shanghai Jiao Tong University School of Medicine, Shanghai, 200336, China.
E-mail addresses: xyliu@mail.sic.ac.cn (X. Liu), lpouyang@shsmu.edu.cn (L. Ouyang), libra_ly@shsmu.edu.cn (Y. Liao).
[1] The authors contributed equally to this work.

https://doi.org/10.1016/j.bioactmat.2022.04.032
Received 22 February 2022; Received in revised form 26 April 2022; Accepted 26 April 2022

of exogenous M2 macrophages, while maintaining M1 macrophages unaffected [10–14]. It is important to suppress pro-inflammatory M1 macrophages for promoting wound healing.

Traditional Chinese medicines have been shown to exhibit immune regulatory effects [15–17]. Puerarin (PUE), a traditional Chinese medicine extracted from the root of kudzu vine, exhibits superior cardioprotective, neuroprotective, and blood glucose levels in diabetes [18–20]. PUE has been reported to possess wound healing activities [21–23]. Recent studies have demonstrated that oral PUE prevents diabetic osteoporosis by suppressing inflammation and apoptosis via HDAC1/HDAC3 signaling [24]. Moreover, oral PUE decreased the levels of TNF-α and IL-6 in the liver [25]. However, only a small portion of PUE is absorbed into the blood and distributed to various tissues and organs because most PUE are metabolized extensively in the liver [26,27]. Low hydrophilicity, poor bioavailability, and low penetration of PUE hinders its application in diabetic wound repair [26,28].

Recently, hydrogels have attracted attention as wound dressings owing to their abundant functional groups, controllable physical properties, natural drug-loading structures, and superior biocompatibility [29–31]. Recent studies have reported that hydrogels have potential applications in the treatment of diabetic [32], burn [33], infected [34], and oral mucosal wounds [35]. Chitosan (CS) is a natural polymer obtained from crabs and shrimp shells and widely used for hydrogel synthesis. Chitosan-based hydrogels are good carriers for drug delivery owing to their nontoxicity, stability, and biodegradability [36–38].

Consequently, a traditional Chinese medicinal hydrogel containing CS and PUE (C@P) was designed to treat diabetic wounds. The promoting effects of the C@P hydrogel on diabetic wound healing and the regulation of inflammatory responses were further explored in type 1 diabetes mellitus (DM) and IL-1β luciferase transgenic mice. miR-29ab1 has been shown to play critical roles in diabetes-related inflammation and macrophage phenotypic switching [39]. Further, miR-29ab1 knockout mice (miR-29ab1$^{-/-}$) were studied to explore the mechanism of C@P in wound healing using histopathology, immunohistochemistry, and quantitative real-time polymerase chain reaction (qRT-PCR) analyses.

2. Materials and methods

2.1. Preparation of the C@P nanofiber hydrogel

The C@P nanofiber hydrogel was fabricated using a one-step grinding process according to the method described in our previous work [40]. First, 70 mg of chitosan (CS; 95% deacetylation degree, 400 mPa s, Aladdin, China) was dispersed in 5 vol% acetic acid (0.5 mL). Another 70 mg of puerarin (PUE; 98% purity, Aladdin, China) was then mixed with chitosan under continuous grinding until a uniform C@P composite was formed, and the solvent was almost evaporated to dry. 1 mL synthetic C@P was injected into 1 mL ultrapure water to test the pH, which was about 6.15. Subsequently, 7 mL of ultrapure water was added to the system to obtain the C @P hydrogel. After grinding for a while until the C@P system became sticky and uniform, the self-assembled C@P hydrogel was collected and left to rest for 24 h at room temperature to ensure a sufficient self-assembly process. The product was then stored at 4 °C for further study. Subsequently, 70 mg of CS or PUE was dispersed in 5 vol% acetic acid (0.5 mL). Then, 7 mL of ultrapure water was added to obtain a CS or PUE solution after continuous grinding to obtain a uniform system.

2.2. Rheological test

The rheological behavior of the C@P nanofiber hydrogel was measured at room temperature using a rheometer (MCR 301; Anton Parr, Austria) with a parallel plate geometry of 25 mm in diameter and a 1 mm gap between plates. A frequency-modulus assay was conducted to study the formation of the C@P hydrogel once the grinding process was stopped. The time-dependent modulus change was recorded during a 3 h modulus test. Meanwhile, 1 mL of well-prepared C@P hydrogel was gently placed at the center of the test plate and allowed to rest for a while. A dynamic frequency sweep test was conducted under a constant strain of 1%. The shear-thinning property of the C@P hydrogel was verified using viscosity measurements at a frequency of 1 Hz. The injectable characterization was assessed by strain sweep measurements over a range of 0.1%–1000% strain. The self-healing ability of the C@P hydrogel was evaluated by a recycled modulus study under a switched strain between 1% and 500%.

2.3. Cell culture and treatment

Mouse mononuclear macrophage leukemia cells (RAW264.7) were provided by the Stem Cell Bank of the Chinese Academy of Sciences. RAW264.7 was cultured in DMEM medium (Gibco, USA) with 15% fetal bovine serum (FBS; Gibco, USA) and 1% penicillin and streptomycin (Antibiotic-Antimycotic; Gibco, USA) in a 37 °C incubator with a humidified atmosphere of 5% CO_2.

Macrophages were seeded in 24-well plates at a density of 1×10^5 cells. After 24 h of culture, 0.5 mL samples (control, CS, PUE, and C@P hydrogel) were placed in transwells and transferred into the plate for another one and 4 days of culture. TRIzol™ reagent (Invitrogen, Thermo Fisher Scientific Inc., USA) was used to extract total RNA from the cells. All solutions containing RNA were collected for qRT-PCR.

2.4. Treatment of animals

All animal experiments were approved and carried out with approval from the Shanghai Tongren Hospital Ethics Committee (2021-090-01).

2.4.1. Murine model of type 1 diabetes mellitus

Intraperitoneal injections of streptozotocin (STZ, 60 mg/kg body weight in 50 mmol/L sodium citrate) for five consecutive days were used to induce a mouse model of diabetes [41–43]. Prior to the first injection, male mice (C57BL/6 weeks) were made to fast for 16 h. Blood glucose was tested after 48 h. Mice were considered diabetic and were used for further study only if they had hyperglycemia (≥16.7 mM).

2.4.2. CRISPR/Cas9-mediated generation of miR-29ab1$^{-/-}$ mice

Previous studies generated homozygous miR-29ab1$^{-/-}$ mice (C57BL/6 strain) using the CRISPR/Cas9 technique [44]. The Shanghai Model Organisms Center (Shanghai, China) provided homozygous mice that were bred for at least four generations to start any experiments.

2.4.3. IL-1β luciferase transgenic mice

The luciferase-2a-egfp-pa expression fragment was inserted into the IL-1β translation initiation site ATG using CRISPR/cas9 technique. IL-1β gene expression in this strain of mice was knocked out, and the endogenous promoter drove the expression of the reporter gene. The intensity of reporter gene expression reflects the degree of activation of IL-1β, which can track the inflammatory factor IL-1β in real-time *in vivo* and visualize the expression pattern of IL-1β [45].

2.4.4. Full-thickness wound model

A mouse model of full-thickness skin wounds was generated in the DM. Sodium pentobarbital (0.1 mg/g of body weight) was administered intraperitoneally to anesthetize the mice, and 75% ethanol was used to sterilize the operating area after shaving the hair on the dorsum. A 10 mm circular (surface area 78.5 mm^2) full-thickness skin wound was created for each animal. Mice were randomly divided into four experimental groups: DM-0 (0.9% NaCl), DM-C (CS), DM-P (PUE), and DM-C@P (C@P). Each wound area was treated with 50 μL of 0.9% NaCl solution, CS solution, PUE solution, or C@P hydrogel, which was injected directly onto the wound surface. The wound areas were then covered with Tegaderm™ dressing (3 M, USA), and the corresponding

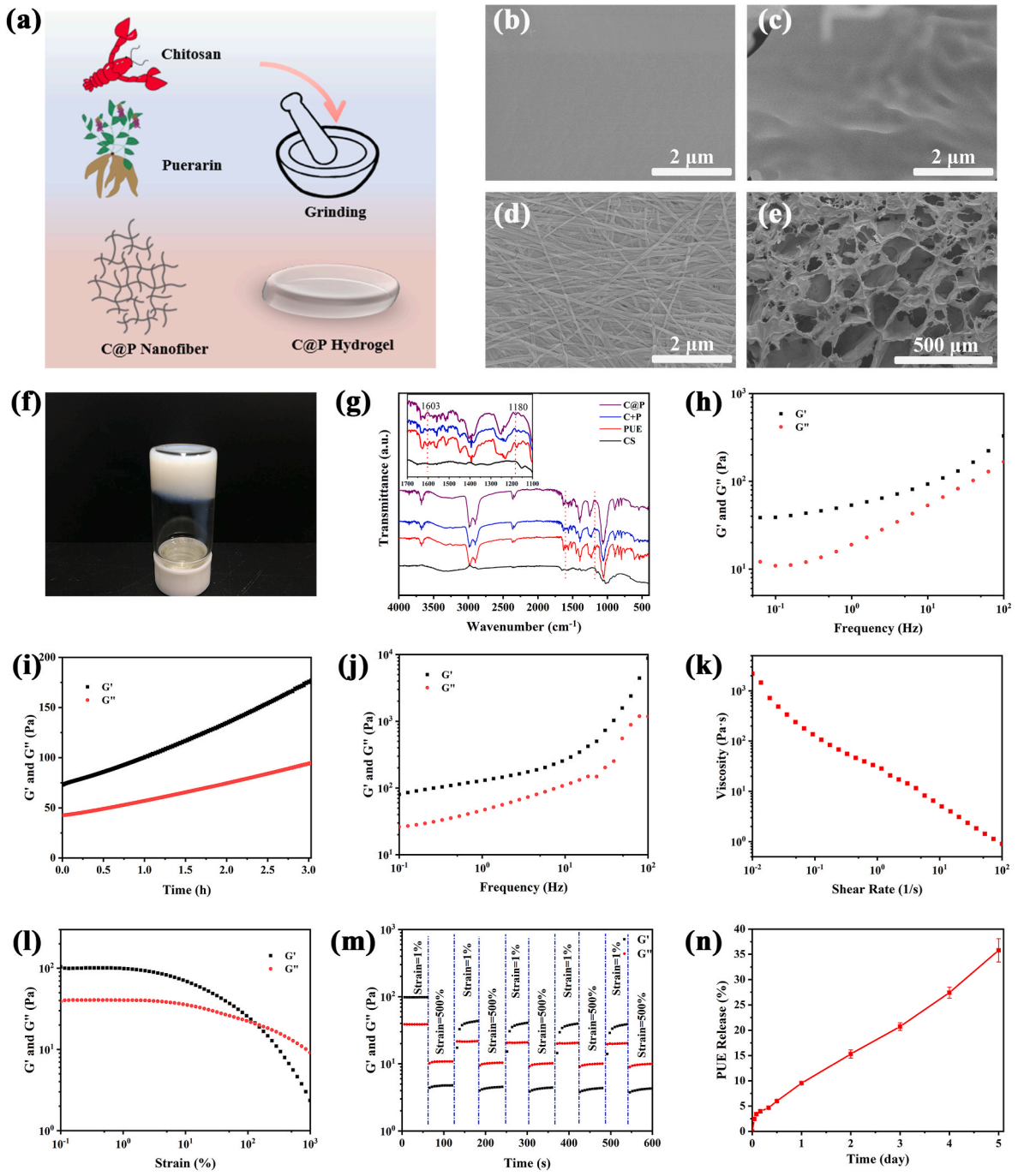

Fig. 1. Synthesis and the characterizations of the C@P hydrogel. Schematic illustration of the synthesis process of the self-assembling nanofiber C@P hydrogel (a). Morphology of chitosan (b), puerarin (c), C@P hydrogel with nanofiber structure (d) and the hydrogel with porous structure (e). Picture of C@P hydrogel at room temperature (f). FTIR spectra of all samples (g). Frequency-dependent rheological behavior of the C@P hydrogel at 1% strain after synthesizing immediately. G': storage modulus, G": loss modulus (h). The change of G′ and G″ under 3 h test (i). Frequency-dependent change in G′ and G″ of the C@P hydrogel in equilibrium statement (g). Shear-thinning property of the hydrogel with the linear relation of viscosity and shear rate (k). Strain-dependent variation of G′ and G" (l). Self-healing property of the hydrogel with the recycle change of strain between 1% and 500% (m). The release of PUE from C@P hydrogel within 5 days (n).

dressing was changed after 7 days. The wound closure rate (%) was determined by measuring the wound area in each group at 7 and 14 days by tracing the wound boundaries using the ImageJ 1.52q software. The following formula was used to calculate wound closure rate (%):

$$\text{Wound closure rate } (\%) = [\text{S (0 day)- S (n day)}]/\text{S (0 day)} \times 100\%, \quad (1)$$

where "n" represents the 7 days or 14 days, and "S" represents the Surface area of the wound section. The wound model described above was also applicable to wild-type (WT) and miR-29ab1$^{-/-}$ mice.

Two 6 mm circular full-thickness wounds of IL-1β luciferase transgenic mice were created after the dorsal hair was shaved and sterilized. Two wounds in each animal were separated from each other as far as possible to avoid crosstalk between the control and C@P groups. A total of 25 μL of 0.9% NaCl solution and C@P hydrogel were injected into two wounds for the same mouse. After 15 min of intraperitoneal injection with luciferin potassium salt (LIFE iLAB BIO, AC19L013), the transgenic mice were anesthetized with isoflurane. Luciferase macroscopic images were captured using a live animal imaging system (Tanon ABL X6,

China) on 0, 1, 3, 5, 7, 10, and 14 days.

2.5. Histopathological and immunohistochemistry analysis of wounds

Each wounded skin sample was divided into two parts. One of them was collected and immediately fixed in a 4% paraformaldehyde solution (PFA, Bio Basic Inc., China). After 24 h, skin wounds were dehydrated overnight and embedded in paraffin. Samples were sectioned transversely to a 5 μm thickness for hematoxylin and eosin (H&E) staining. Additionally, skin wounds in paraffin blocks were sliced, and VEGF was labeled immunohistochemically (Servicebio, gb13034, 1:300). Rabbit polyclonal anti-collagen type I (Col I, Servicebio, gb11022-3, 1:1000) and rabbit polyclonal anti-collagen type III (Col III, Servicebio, gb111629, 1:500) were used as markers for collagen deposition. Rabbit polyclonal anti-F4/80 (Servicebio, gb11027, 1:1000) was used as the macrophage marker. Rabbit polyclonal anti-lL-1β (Servicebio, gb11113, 1:200) and rabbit polyclonal anti-TNF-α (Servicebio, gb11188, 1:200) were used as markers of pro-inflammatory cytokines.

To detect the type of macrophage, skin wounds in paraffin blocks were sliced and treated with citric acid repair solution (Servicebio, g1202, pH 6.0) for antigen retrieval. To test the specificities of inducible nitric oxide synthase (iNOS) for M1 macrophages and CD206 for M2 macrophages, some tissue sections were incubated with iNOS/CD206 and/F4/80, then added the corresponding secondary antibody. The double label results showed that iNOS and CD206 have specificities for M1 and M2 respectively (Fig. S1). The other tissue sections were then incubated with rabbit polyclonal anti-iNOS antibody (NOVUS, nb300-605, 1:50) for M1 macrophages and mouse polyclonal anti-CD206 antibody (RD, af2535, 1:200) for M2 macrophages, overnight. Secondary antibodies of Cy3 conjugated donkey anti-rabbit IgG (Servicebio, gb21403, 1:300) and FITC conjugated donkey anti-goat IgG (Servicebio, gb22404, 1:200) were treated for the primary antibodies.

2.6. Quantitative real-time PCR

Skin from the other wound was collected and analyzed by qRT-PCR for miR-29a/b1 expression. Total RNA was extracted with TRIzol™ reagent, and cDNA was synthesized by reverse transcription. The cDNA served as a template for qRT-PCR performed using a real-time PCR (QuantStudio 3 Real-Time PCR System, ABI, USA). Genes were analyzed using U6 spliceosomal RNA (U6) as a housekeeping gene for normalization and relative quantification. Primer sequences are listed in Table S1 qRT-PCR experiments were performed at least twice, and each sample was analyzed in duplicate. The relative expression was quantified using the comparative threshold method. Solutions with RNA from macrophages were collected and detected by qRT-PCR for miR-29a/b1 expression, as described above.

2.7. Statistical analysis

All statistical analyses were performed using the GraphPad Prism software (GraphPad 9.0, USA). Results are presented as mean ± standard error of the mean (SEM). An unpaired two-tailed *t*-test was used to analyze the significant differences between groups, and a p-value of less than 0.05 was considered statistically significant.

3. Results

3.1. Characterization of C@P hydrogel

CS and PUE are the active ingredient extracts of chitin and Pueraria, respectively, which are valued natural products. Inspired by the facile preparation method of traditional Chinese medicine, grinding was conducted to synthesize the C@P nanofiber hydrogel, as shown in Fig. 1a. The distinct entangled nanofiber structure of the C@P hydrogel with a diameter of 50–100 nm was confirmed by SEM imaging, whereas the morphology of CS and PUE was smooth and plain (Fig. 1b–d). Meanwhile, a comparison of the appearance and morphology of the puerarin and chitosan (C + P) mixture and C@P hydrogels showed that the C + P mixture was light white and exhibited a solid state, while C@P was milky and presented a hydrogel state. Moreover, large quantities of nanofibers were observed in the C@P hydrogel, while the morphology of C + P was smooth and the nanofiber structure could not be seen in C + P, which was similar to CS and PUE (Fig. S2). The nanofiber structure of the C@P hydrogel may originate from the self-assembly process induced by the interaction of hydrogen bonds and π–π bonds between the PUE and CS solutions. Accompanied by the evolution of self-assembly, the typical porous structure of the hydrogel appeared, and the C@P hydrogel was built, as shown in Fig. 1e and f. Interactions between CS and PUE were further confirmed using FTIR spectroscopy (Fig. 1g). Compared to the FTIR spectrum of the CS and PUE mixture, the absorption peak at approximately 1603 cm^{-1} of the C@P hydrogel disappeared. This absorption peak corresponds to the C═O vibration of PUE, and a large number of hydrogen bonds in the C@P hydrogel influenced the C═O stretching, which further resulted in a change in the corresponding peak. In addition, the absorption peak at 1173 cm^{-1} of PUE, which is related to C–O vibration, shifted toward a higher wavenumber (i.e., 1180 cm^{-1}) after assembly with CS. The change in C–O could be attributed to the physical interaction of the CS chain and PUE induced by hydrogen bonds during hydrogel formation.

3.2. Rheological properties of C@P hydrogel

Owing to the irregular shape of diabetic wounds, an injectable hydrogel with self-healing ability is preferred. Herein, the rheological properties reflected by the changes in the storage modulus (G′) and loss modulus (G″) of the C@P nanofiber hydrogel were inspected. To investigate the formation speed of the C@P hydrogel, G′ and G″ were tested once the grinding was stopped. The initial storage modulus G' = 38.5 Pa, which was greater than the loss modulus G'' = 12.1 Pa, indicating that the hydrogel was formed during the grinding process (Fig. 1h). The time-dependent modulus change was also studied to verify the constant self-assembly of the hydrogel after its formation. G′ increased from 72.7 Pa to 178 Pa, and G″ increased from 42.6 Pa to 95.3 Pa under 1% strain and 1 Hz frequency (Fig. 1i). The increase in the modulus indicated that self-assembly induced by hydrogen bonds was a continuous process. The dynamic frequency sweep test of the hydrogel was conducted while the C@P hydrogel was left resting and maintained an equilibrium state. The result in Fig. 1j shows the formation and stable state of the hydrogel with a G′ of 100 Pa and a relatively small G′ of 20 Pa under low frequency. G′ and G″ apparently increased with increasing frequency. The negative correlation between the viscosity and shear rate shown in Fig. 1k indicates the shear-thinning behavior of the C@P hydrogel, ensuring the injectable property of the resulting hydrogel. Moreover, based on the result of the intersection point of G' and G" under 100% strain in Fig. 1l, which could be related to the network failure of the C@P hydrogel, a recycled oscillatory strain between 500% and 1% strain was applied to break and recover the hydrogel structure. Results in Fig. 1m demonstrate that the broken structure of the C@P hydrogel could recover quickly and maintain the hydrogel state over five cycles. Moreover, 2 mL of the C@P hydrogel was injected on a plate, and the hydrogel (0.5 mL) was removed, leaving a hole. Subsequently, a fresh 0.5 mL of C@P hydrogel was injected into the hole and the incomplete C@P hydrogel recovered, further indicating the self-healing ability of the C@P hydrogel (Fig. S3).

The swelling ratios of the C@P hydrogels were tested using immersion methods. The swelling ratios were 129.1%, 154.9%, and 189.6% at 12, 24, and 48 h, respectively (Fig. S4). The swelling behavior of the C@P hydrogels was further assessed by changes in appearance and morphology. The appearance of the swollen hydrogel was similar to that of the original hydrogel. The viscosity decreased due to the expansion of the volume, and the C@P hydrogel could still be inverted after swelling.

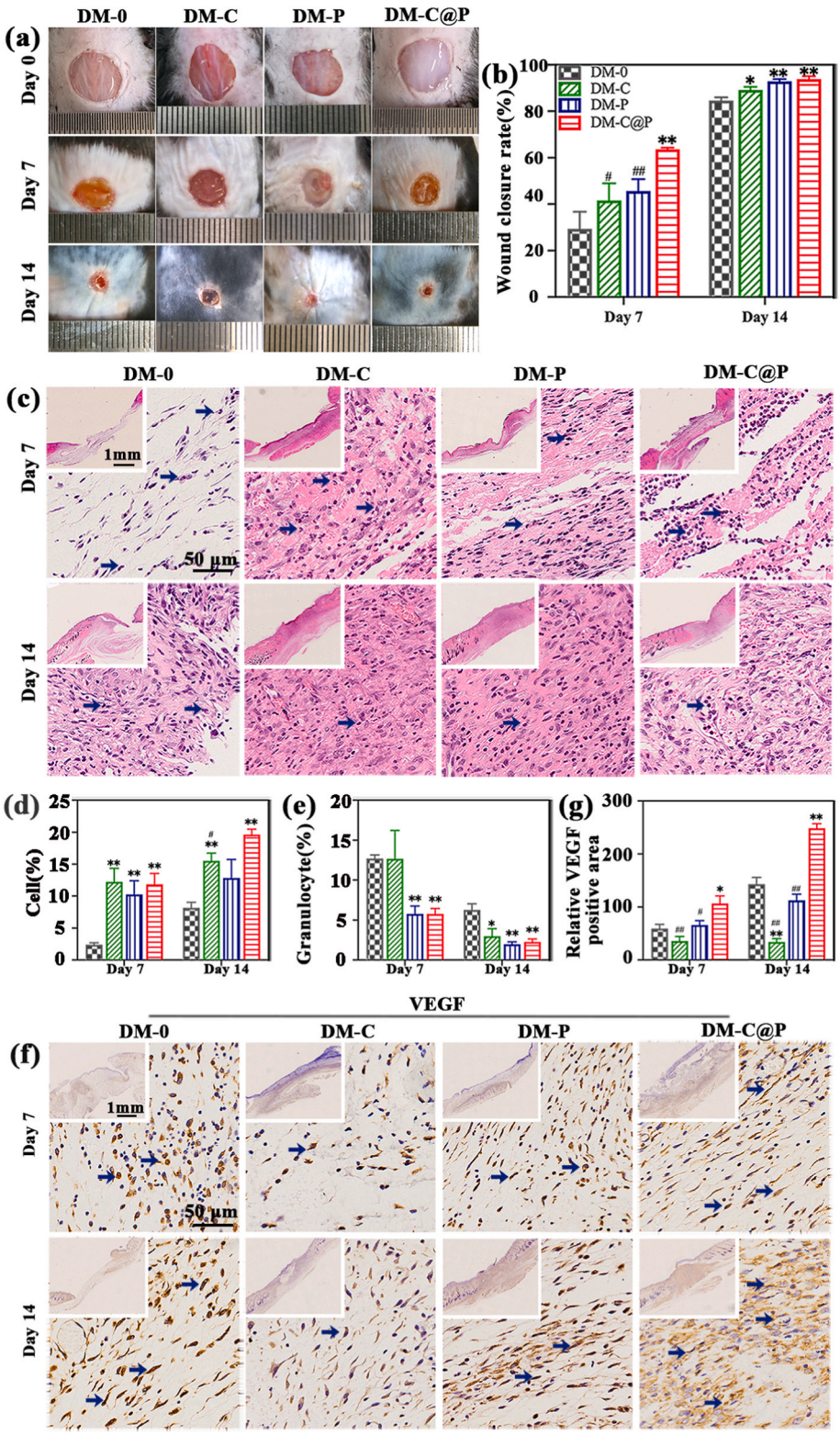

Fig. 2. C@P hydrogel promoted wound healing of chronic wounds in DM. Representative images of the wound healing process were taken at 0 day, 7 days, and 14 days after wounding *in vivo*. Scale bar, 20 mm (a). Wound closure rate (%) was determined at 7 days and 14 days. The rates are presented as a percentage of the initial wound area at 0 day, 7 days, and 14 days (n = 5, b). Full-thickness skin samples containing entire wound sites were stained with H&E at 7 days and 14 days, granulocytes (blue arrow, c). Scale bar, 1 mm and 50 μm. Quantification of cell density at 7 days and 14 days (n = 5, d). Quantitative analysis of the granulocytes at 7 days and 14 days (n = 5, e). Representative images of VEGF (blue arrow) immunohistochemical staining labeling of the regenerated wound tissue at 7 days and 14 days. Scale bar, 1 mm and 50 μm (f). Quantitative analysis of the VEGF at 7 days and 14 days (n = 4, g). Data are presented as the means ± SEM. *$p < 0.05$ and **$p < 0.01$ compared with DM-0 group; $^{\#}p < 0.05$ and $^{\#\#}p < 0.01$ compared with DM-C@P group. (For interpretation of the references to colour in this figure legend, the reader is referred to the Web version of this article.)

Moreover, the swollen C@P hydrogel presented a porous nanofiber morphology similar to that of the original C@P hydrogel (Fig. S5). The degradation of the C@P hydrogel was assessed *in vitro* and is shown in Fig. S6. The degradation rate of the hydrogel reached 74% in a week, illustrating its excellent degradation behavior. The nearly linear release behavior of PUE proved that the C@P hydrogel could sustain a constant release of PUE in 5 days (Fig. 1n). PUE was released not only from the hydrogel nanofiber structure, but also during the degradation process. The total amount of PUE released after five days was less than 40%. Therefore, the sustained release of PUE from the C@P hydrogel improved the bioavailability of PUE and ensured its biocompatibility. Several experiments, including CCK8 assay and LIVE/DEAD staining, were conducted to assess the biocompatibility of the C@P hydrogel. As illustrated in Fig. S7, there was no significant difference in cell viability

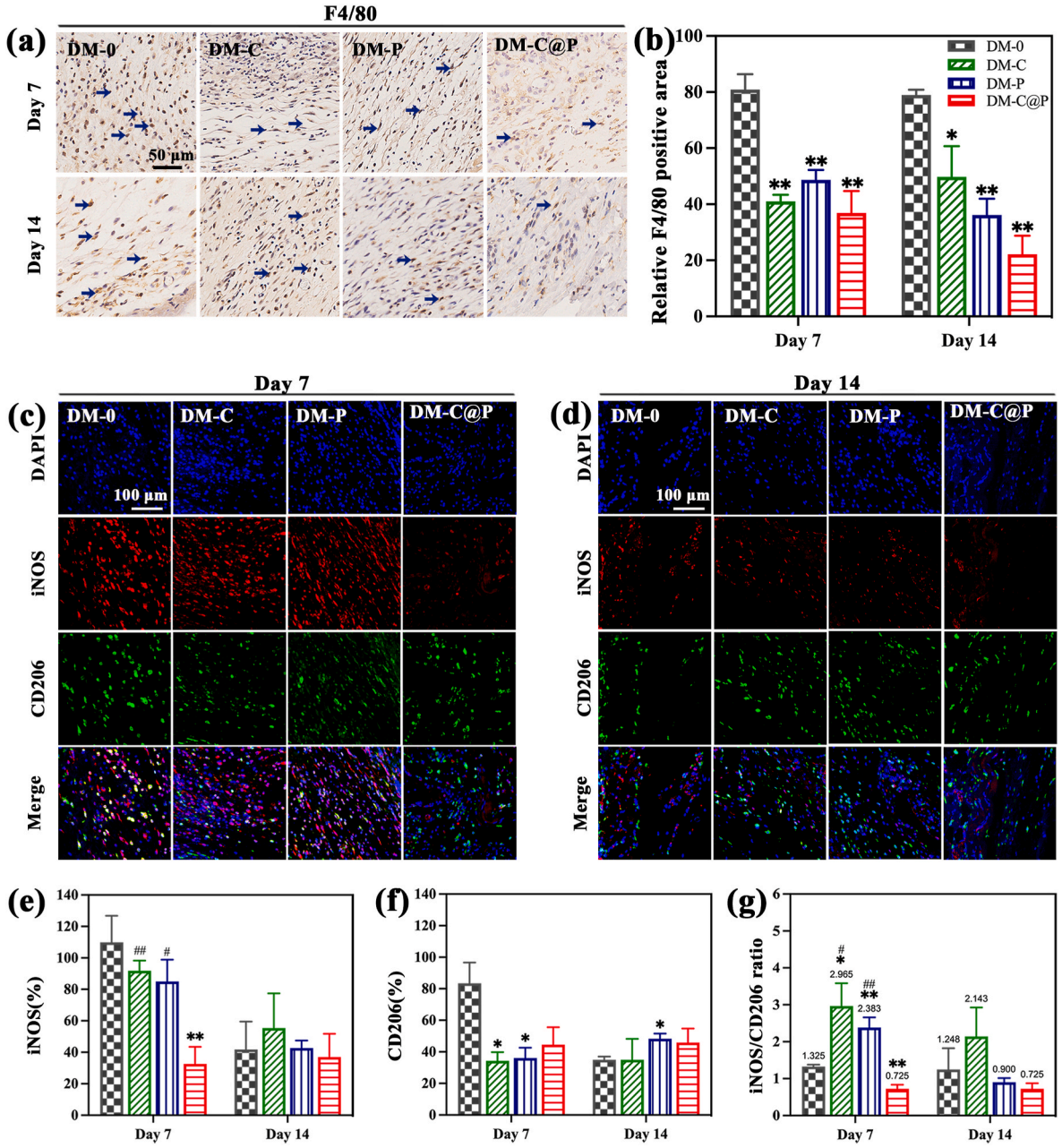

Fig. 3. C@P hydrogel inhibited M1 macrophage expression. Representative immunohistochemical staining images of wound bed with F4/80 (blue arrow) were taken at 7 days and 14 days. Scale bar, 50 μm (a). Quantitative analysis of F4/80 expression at 7 days and 14 days (n = 4, b). Representative immunofluorescence staining of iNOS (M1 macrophage) and CD206 (M2 macrophage) in wound bed at 7 days (c) and 14 days. Scale bar, 100 μm (d). Quantitative analysis of iNOS at 7 days and 14 days (n = 4, e). Quantitative analysis of CD206 at 7 days and 14 days (n = 4, f). iNOS/CD206 ratio at 7 days and 14 days (n = 4, g). Data are presented as the means ± SEM. *$p < 0.05$ and **$p < 0.01$ compared with the DM-0 group; $^{\#}p < 0.05$ and $^{\#\#}p < 0.01$ compared with the DM-C@P group. (For interpretation of the references to colour in this figure legend, the reader is referred to the Web version of this article.)

at 24 and 48 h between each group, which was associated with the excellent biocompatibility of CS and PUE as natural polymers and natural traditional Chinese medicine, respectively. Results of LIVE/DEAD staining revealed that the cells co-cultured with each sample exhibited an ultrahigh survival rate, further illustrating the excellent biocompatibility of the C@P hydrogel.

3.3. C@P hydrogel accelerated diabetic wound healing

A full-thickness skin wound model in DM mice was used to assess the effect of the C@P hydrogel on diabetic wound healing. Digital photographs were obtained 0, 7, and 14 days after surgery (Fig. 2a). The wound area was measured to quantify the wound healing speed, and the wound closure rate (%) as shown in Fig. 2b. The wound closure rate (%) of the DM-C@P group was significantly higher than that of the DM-0 group on 7 and 14 days ($p < 0.01$). Compared to the DM-C and DM-P groups at day 7, the wound closure rate (%) of the DM-C@P group was markedly increased ($p < 0.05$, $p < 0.01$).

To further estimate the capability of the C@P hydrogel to promote healing, H&E and immunohistochemical staining of VEGF, Col I and Col III were used to analyze the tissue sections of the wound bed at 7 and 14 days. As shown in Fig. 2c, the wound bed of the C@P-treated mice presented thicker skin structures than other groups at 7 days, and the wound length of the C@P-treated group was shorter than that of other

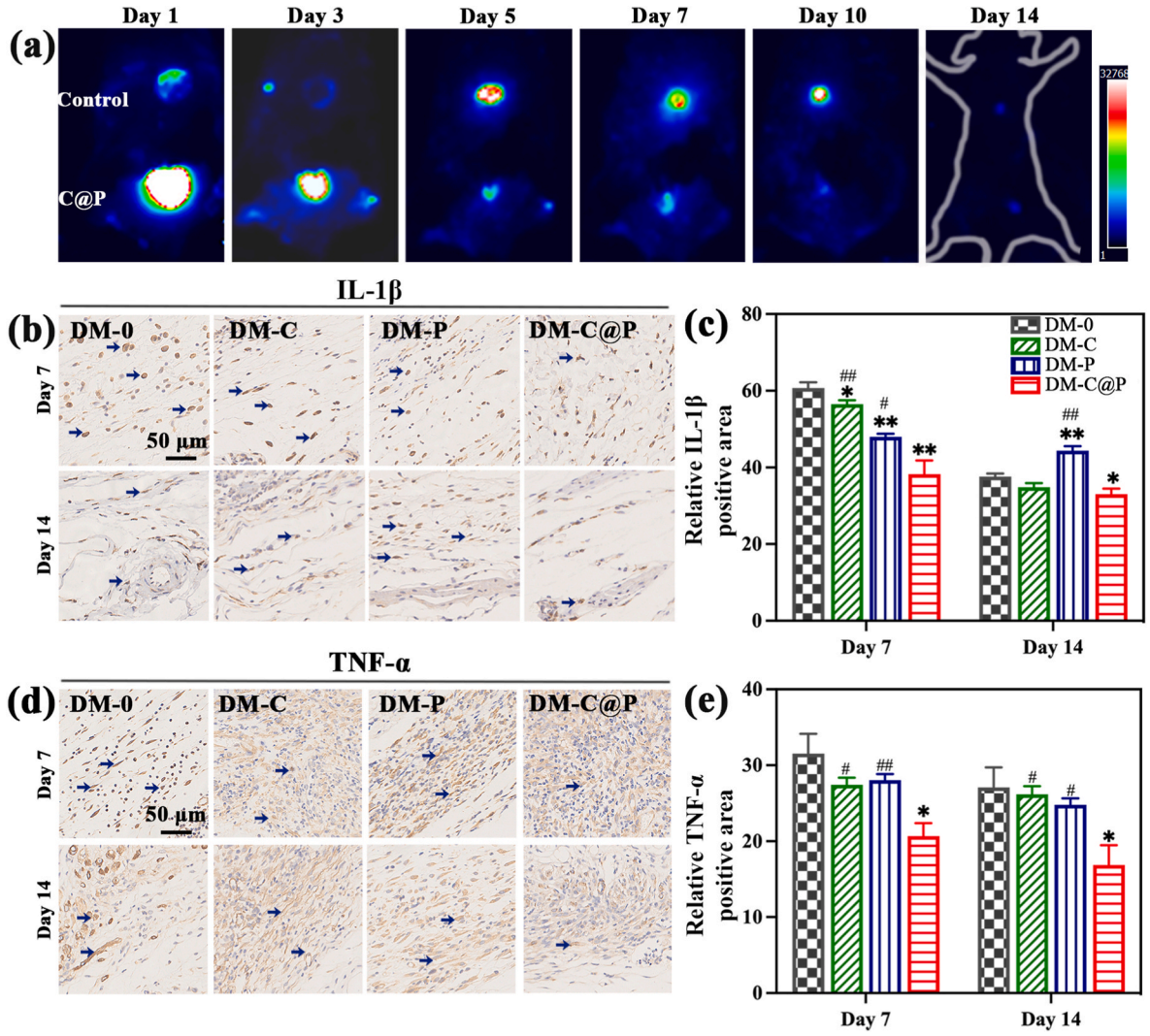

Fig. 4. C@P hydrogel inhibited the IL-1β and TNF-α expression of wound bed. IL-1β was tracked in real time on wound bed of IL-1β luciferase transgenic mice, and images of wound bed showed the dynamic IL-1β expression at 1 day, 3 days, 5 days, 7 days, 10 days, and 14 days (a). Representative images of IL-1β (blue arrow) were taken at 7 days and 14 days. Scale bar, 50 μm (b). Quantitative analysis of IL-1β (n = 5, c). Representative images of TNF-α (blue arrow) were taken at 7 days and 14 days. Scale bar, 50 μm (d). Quantitative analysis of TNF-α at 7 days and 14 days (n = 4, e). Data are presented as the means ± SEM. *$p < 0.05$ and **$p < 0.01$ compared with the DM-0 group; $^{\#}p < 0.05$ and $^{\#\#}p < 0.01$ compared with the DM-C@P group. (For interpretation of the references to colour in this figure legend, the reader is referred to the Web version of this article.)

groups at 14 days. The cell density of the C@P-treated group was significantly higher than that of the DM-0 group at both 7 and 14 days ($p < 0.01$). Meanwhile, the cell density of DM-C@P was enhanced significantly, even when compared with that of the DM-C group at 14 days ($p < 0.05$, Fig. 2d). The granulocytes (%) of the treatment areas collected from C@P-treated mice were effectively suppressed at 7 and 14 days compared to that of the control group ($p < 0.01$, Fig. 2e). VEGF is a key cytokine involved in angiogenesis. As shown in Fig. 2f and g, VEGF expression in the DM-C@P group was significantly higher than that in the DM-0, DM-C, and DM-P groups at both 7 and 14 days ($p < 0.05$, $p < 0.01$). The collagen level is essential for new capillary formation. Representative immunohistochemistry images of Col I demonstrated that the Col I expression of C@P-treated mice was amplified at 7 and 14 days compared to that in the DM-0 group (Fig. S8a), and the increase in Col I of the DM-C@P group was statistically significant compared to that in the DM-0 group at 14 days ($p < 0.05$). However, Col I expression in the DM-C group was significantly lower than that in the DM-0 group at 7 and 14 days ($p < 0.01$, $p < 0.05$, respectively), and Col I expression in the DM-P group was significantly lower than that in the DM-0 group at 14 days ($p < 0.01$, Fig. S8b). The representative images showed that the DM-C@P group had a massive Col III positive area (Fig. S8d), and Col III expression in C@P-treated mice was increased at 7 and 14 days compared to that in the DM-0 group (Fig. S8c, $p < 0.01$, $p < 0.05$). Consequently, the C@P hydrogel accelerates wound repair and angiogenesis.

3.4. C@P hydrogel inhibited inflammation

In the early wound healing stage, macrophages respond to inflammatory cells [46]. F4/80 is a mature mouse macrophage marker, and macrophages were examined by immunohistochemistry of the cell marker F4/80 at 7 and 14 days (Fig. 3a and b). Representative images at high magnification showed that there was an enormous F4/80 positive area in the DM-0 group. The F4/80-positive staining areas in the wound beds of DM-C, DM-P, and DM-C@P were lower than those in DM-0 at both 7 and 14 days ($p < 0.05$, $p < 0.01$). DM-C@P exhibited the lowest F4/80 expression at 7 days and 14, indicating minimal macrophages in the wound area. iNOS and CD206 are functional markers of the M1 and M2 phenotypes respectively [47–49]. As shown in Fig. 3c–g, immunofluorescence of iNOS and CD206 in the wound bed was observed at 7

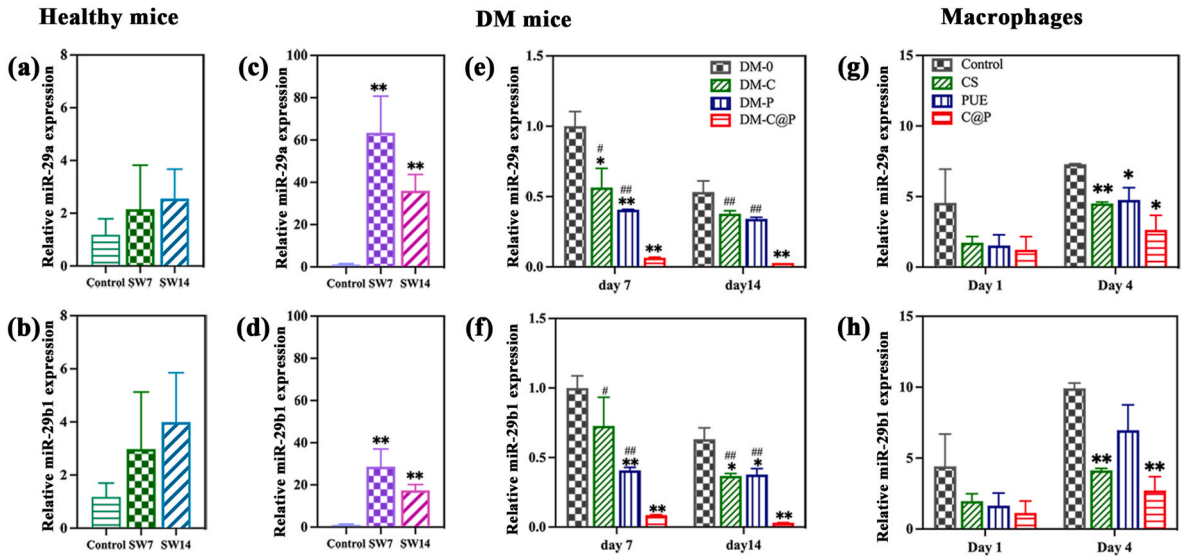

Fig. 5. C@P inhibited miR-29a/b1 expression which was ectopic increased in diabetic wound healing. Relative miR-29a/b1 expression in wound bed of healthy mice (n = 5, a, b) Relative miR-29a/b1 expression in diabetic wound (n = 5, c, d). Relative miR-29a/b1 expression in wound bed of DM-0 group, DM-C group, DM-P group, and DM-C@P group at 7 days and 14 days (n = 4, e, f). Relative miR-29a/b1 expression in macrophages (n = 3, g, h). Data are presented as the means ± SEM. *p < 0.05 and **p < 0.01 compared with the control group or DM-0 group; $^{\#}$p < 0.05 and $^{\#\#}$p < 0.01 compared with DM-C@P group.

and 14 days. iNOS expression in the wound bed of C@P-treated mice was threefold compared to that in the DM-0 group at 7 days (p < 0.01). Compared with the DM-C and DM-P groups at 7 days, iNOS expression in the wound bed of the DM-C@P group was significantly reduced (p < 0.01, p < 0.05). CD206 expression in the wound bed of DM-0 mice decreased progressively from day 7 to day 14. CD206 expression in the DM-C@P group was reduced, with no significant difference at 7 days, and slightly elevated at 14 days compared with DM-0 mice. However, CD206 expression in the DM-C and DM-P groups was significantly reduced at 7 days compared to that in the DM-0 group (p < 0.05). The iNOS/CD206 ratio of the DM-C@P group (0.725) at 7 days was significantly lower (p < 0.05) compared with iNOS/CD206 ratio of the DM-0 group at 7 days (1.325). Conversely, compared with the iNOS/CD206 ratio of the DM-0 group at 7 days, the ratio of the DM-C (2.965) and DM-P (2.383) groups was significantly elevated (p < 0.05, p < 0.01). Moreover, the iNOS/CD206 ratio expression in the four groups at 7 days was reduced compared to that at 14 days. Overall, the C@P hydrogel reduced the number of macrophages and inhibited the polarization of M1 macrophages in the diabetic wounds.

Macrophages play important roles in the progression of diabetes, which is sustained by chronic inflammation, and M1 macrophages produce and secrete higher levels of the pro-inflammatory cytokines IL-1β and TNF-α [50]. IL-1β luciferase transgenic mice were used to observe the dynamic expression of IL-1β in the control and C@P groups for 14 days. Although the fluorescence intensity of the wound bed collected from the C@P group was higher than that of the control group at 1 and 3 days, it was markedly lower than that of the control group at 5, 7, 10, and 14 days (Fig. 4a). After 10 days, the control group showed strong fluorescence emission. Immunohistochemical staining was used to assess IL-1β expression in the wound bed. Statistical results showed that IL-1β expression in the wound bed of C@P-treated mice dropped dramatically at 7 days and 14 compared to that in the DM-0 group. IL-1β expression in the wound bed from the C@P-treated group was significantly inhibited compared to that in the DM-C or DM-P groups at 7 days (Fig. 4b and c). TNF-α expression in the wound bed of the C@P-treated group was significantly reduced compared to that in the wound bed of the DM-0 group at 7 and 14 days (p < 0.05). TNF-α expression in DM-C@P mice was markedly reduced at 14 days compared with that in DM-C or DM-P mice (p < 0.05, p < 0.01, Fig. 4d and e).

3.5. *miR-29ab1*$^{-/-}$ *and diabetic wound inflammation*

Based on our previous work, miR-29 is closely associated with inflammatory responses and angiogenesis [44,51]. miR-29a/b1 accumulation in the healthy skin wound at 0, 7, and 14 days (Control, HL-SW7, and HL-SW14) was evaluated and showed no notable relationship with the wound healing process (Fig. 5a and b). However, miR-29a/b1 expression was significantly increased in diabetic skin wounds at 0, 7, and 14 days (p < 0.01, Control, DM-SW7, and DM-SW14, Fig. 5c and d). Relative miR-29a/b1 expression in newborn skin collected from DM-C@P decreased significantly at 7 and 14 days compared with that from DM-0 mice (p < 0.01, Fig. 5e and f). Compared with the relative miR-29a/b1 expression in the DM-C or DM-P groups, the relative miR-29a/b1 expression in the DM-C@P group decreased significantly at 7 and 14 days (p < 0.05, p < 0.01). *In vitro* experiments, relative miR-29a/b1 expression in CS-treated, PUE-treated, and C@P-treated macrophages was reduced slightly at 1 day compared with the control group. Moreover, relative miR-29a/b1 expression in C@P-treated macrophages was markedly downregulated compared with that in the control group at 4 days (p < 0.05, p < 0.01, Fig. 5g and h). Hence, the above results suggest that miR-29ab1 was tightly linked with the diabetic wound, and the C@P hydrogel accelerated the healing process by inhibiting ectopic high miR-29ab1 expression.

To further verify the regulation of miR-29ab1 in inflammation and wound healing, miR-29ab1$^{-/-}$ mice were used to create the full-thickness skin wound. The skin wound area of miR-29ab1$^{-/-}$ mice got smaller than that of WT mice at 7 and 14 days from the presented images (Fig. 6a). miR-29ab1$^{-/-}$ mice exhibited improved wound closure rates (%) and shorter wound length compared with WT mice, accompanied by pronounced increases in cell density of the wound bed at 7 and 14 days (Fig. 6b–d). However, the number of granulocytes concomitantly decreased in miR-29ab1$^{-/-}$ mice compared with that in WT mice (Fig. 6e). VEGF and Col I expression in WT mice and miR-29ab1$^{-/-}$ mice were further subjected to extensive histomorphometric analyses, and results revealed that VEGF and Col I expression in miR-29ab1$^{-/-}$ mice was significantly higher than that in WT mice at 7 days and 14 days (Fig. 6f–i). Therefore, miR-29ab1$^{-/-}$ mice presented excellent wound healing and angiogenesis compared to WT mice.

To further understand the role of miR-29ab1 on macrophage phenotypes in skin wound healing, the expression of F4/80, iNOS, and

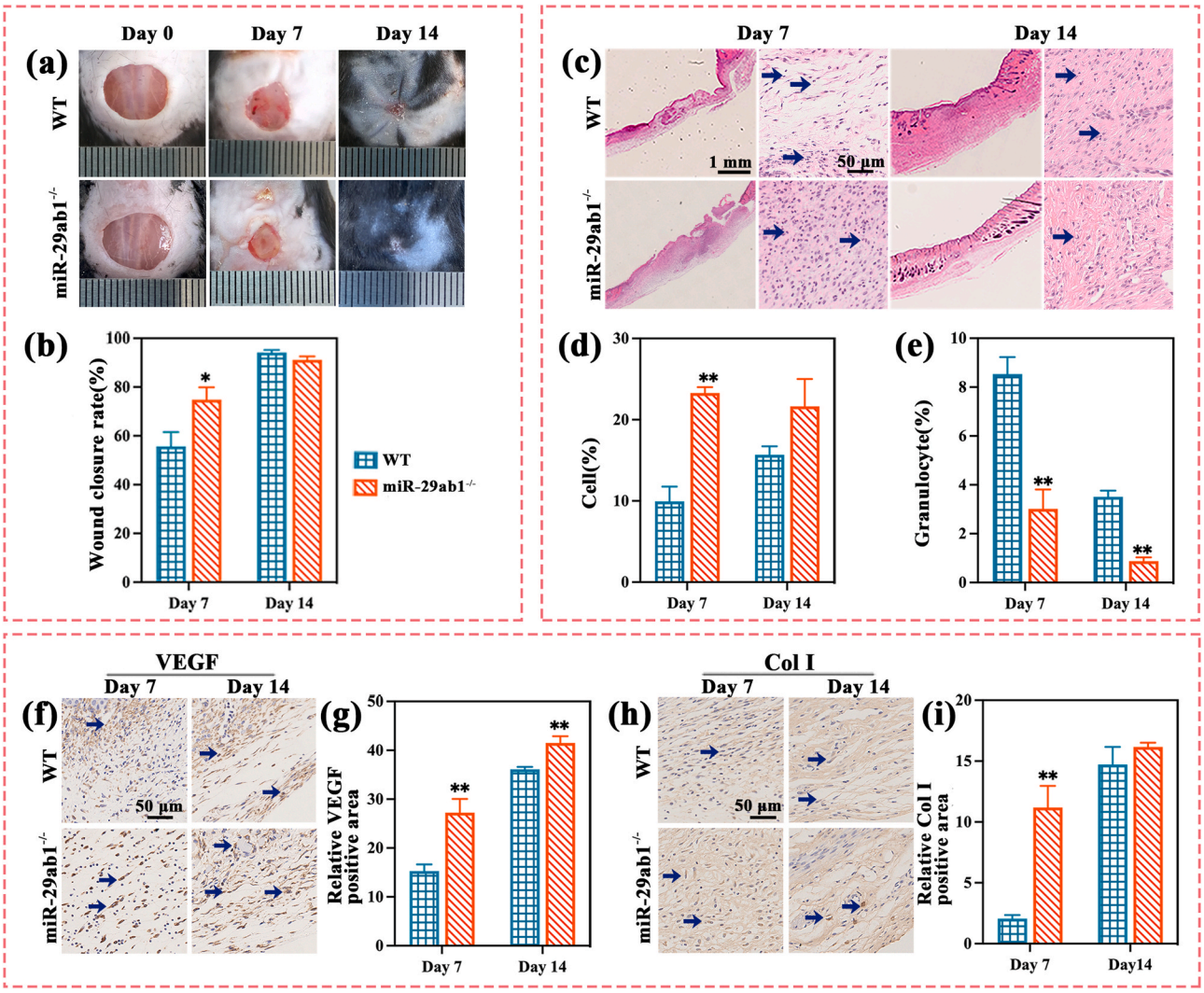

Fig. 6. miR-29ab1$^{-/-}$ mice promoted regenerative wound healing, increased angiogenesis and promoted collagen synthesis. Representative images of the wound closure process were taken at 0 day, 7 days, and 14 days after wounding *in vivo*. Scale bar, 20 mm (a). Wound closure rate (%) was determined at 7 days and 14 days (n = 5, b). Full-thickness skin samples containing entire wound sites were stained with H&E at 7 days and 14 days, granulocytes (blue arrow, Scale bar, 1 mm and 50 μm c). Quantification of cell density at 7 days and 14 days (n = 4, d). Quantitative analysis of the granulocytes at 7 days and 14 days (n = 4, e). Representative images of VEGF (blue arrow) were taken at 7 days and 14 days. Scale bar, 50 μm (f). Quantitative analysis of VEGF at 7 days and 14 days (n = 5, g). Representative images of Col I (blue arrow) were taken at 7 days and 14 days. Scale bar, 50 μm (h). Quantitative analysis of the Col I at 7 days and 14 days (n = 4, i). Data are presented as the means ± SEM. *p < 0.05 and **p < 0.01 compared with the WT group. (For interpretation of the references to colour in this figure legend, the reader is referred to the Web version of this article.)

CD206 was evaluated using immunohistochemistry analysis (Fig. 7a–h). Compared to WT mice, F4/80 expression of miR-29ab1$^{-/-}$ mice in wound bed was decreased significantly at 14 days and decreased slightly at 7 days. Immunofluorescence staining demonstrated that iNOS expression in the wound bed of miR-29ab1$^{-/-}$ mice was lower than that in WT mice at 7 and 14 days. CD206 expression in the wound bed of miR-29ab1$^{-/-}$ mice was slightly reduced at 7 and 14 days compared to that in the WT mice. Compared to the iNOS/CD206 ratio of WT mice at 14 days, the ratio of miR-29ab1$^{-/-}$ mice was significantly reduced ($p < 0.01$). The statistical results showed that IL-1β (Fig. 7i and j) and TNF-α (Fig. 7k and l) expression in miR-29ab1$^{-/-}$ mice was lower than that in WT mice.

4. Discussions

Macrophages play a critical role in wound healing. In healthy wounds, macrophages are capable of phagocytosis of dead granulocytes, thus promoting an M1-M2 macrophages phenotypic switch [52]. Diabetes mellitus is a chronic inflammatory disease [53]. Pro-inflammatory macrophages (M1) persist in the long term without transitioning to an anti-inflammatory phenotype (M2) in chronic DM wounds, which is considered to result in sustained inflammation and impaired tissue repair [54–57]. Research has shown that a decreased ratio of M1/M2 macrophages correlates with biomaterial vascularization [8]. Thus, correcting prolonged inflammation and suppressing excessive M1 macrophages in DM wounds were the main research objectives of the current study.

Various methods can be used to regulate inflammation and macrophage orchestration. Chemical composition and structure construction are two types of methods that can be applied to regulate macrophage activation. Shape, stiffness, and surface properties are physical factors that influence inflammation and macrophage activation. Increased expression of arginase 1 (Arg-1) along with a decrease in iNOS occurs in materials with large fibers, which is beneficial from the infiltration and natural spread-out morphology [58]. In addition to physical factors, chemical signals can affect macrophage activation. Metal ions, such as

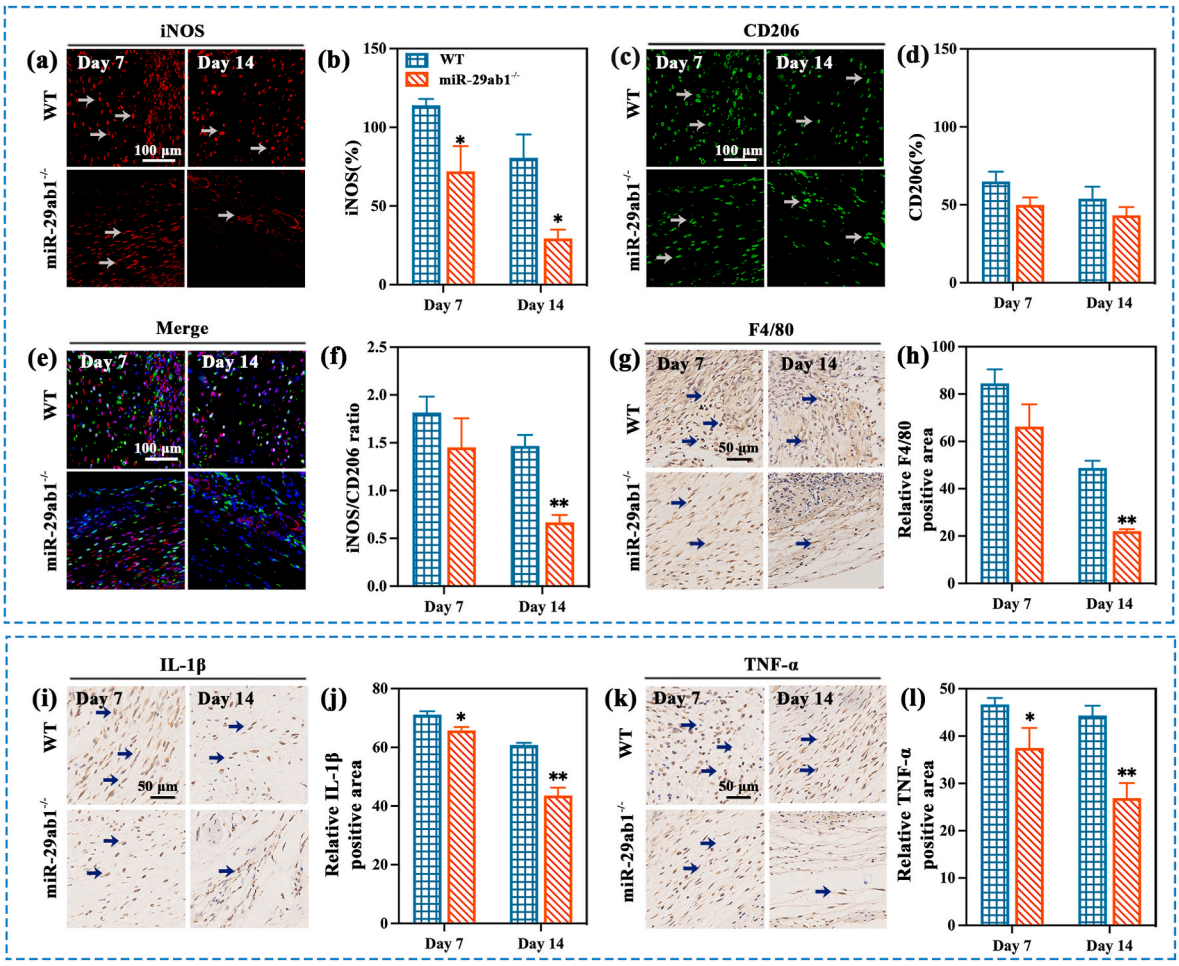

Fig. 7. miR-29ab1$^{-/-}$ mice inhibited inflammation response via suppressing inflammation. Representative images of iNOS (white arrow) were determined at 7 days and 14 days. Scale bar, 100 μm (a). Quantitative analysis of iNOS at 7 days and 14 days (n = 5, b). Representative images of CD206 (white arrow) were determined at 7 days and 14 days. Scale bar, 100 μm (c). Quantitative analysis of CD206 at 7 days and 14 days (n = 5, d). Representative images of merge. Scale bar, 100 μm (e). Quantitative analysis of iNOS/CD206 ratio at 7 days and 14 days (n = 5, f). Representative images of F4/80 (blue arrow) were taken at 7 days and 14 days. Scale bar, 50 μm (g). Quantitative analysis of F4/80 at 7 days and 14 days (n = 4, h). Representative images of IL-1β (blue arrow) were taken at 7 days and 14 days. Scale bar, 50 μm (i). Quantitative analysis of IL-1β (n = 5, j). Representative images of TNF-α (blue arrow) were taken at 7 days and 14 days. Scale bar, 50 μm (k). Quantitative analysis of TNF-α at 7 days and 14 days (n = 5, l). Data are presented as the means ± SEM. *p < 0.05 and **p < 0.01 compared with the WT group. (For interpretation of the references to colour in this figure legend, the reader is referred to the Web version of this article.)

zinc, magnesium, and calcium, are known to promote M2 macrophage activation at appropriate concentrations [59]. Traditional Chinese medicine is receiving increasing attention because of its superior ability to regulate the immune response [60,61]. PUE exhibits multiple pharmacological activities such as antioxidant and anti-inflammatory activities [62], collagen production [63] and attenuation of insulin resistance [18,64]. Chitosan-based hydrogels have been shown to accelerate diabetic wound healing by inhibiting excessive inflammation [65–67]. In this study, a C@P hydrogel with a nanofiber structure was constructed, and the results showed that C@P hydrogel could improve diabetic wound healing by suppressing inflammatory reactions and regulating macrophage activation. These beneficial effects may be attributed to both physical and chemical clues. On the one hand, nanofiber-like C@P provided a good texture for macrophage filtration and spread, thus accelerating M1 suppression, while the C@P hydrogel exhibited multiple pharmacological activities, including anti-inflammatory and macrophage regulation.

The miR-29 family members play critical roles in diabetes and inflammation because of their direct involvement in regulating insulin secretion by β cells as well as macrophage inflammatory tone. The type 1 diabetic mouse model, associated with insulitis, shows enhanced expression of miR-29 in β cells [68], and β cell-derived exosome miR-29 is transcellularly transported into circulating monocytes/macrophages with diabetes progression [39]. Interestingly, miR-29 is among the most highly expressed microRNAs in the pancreas [69] and is expressed at low levels in the intact skin [44,70]. Therefore, miR-29ab1 expression in normal skin of healthy and diabetic mice did not differ. However, the upregulation of miR-29a and miR-29b1 was induced by full-thickness wound stimuli. miR-29a/b1 showed a slight increase in wounded skin compared to intact skin in healthy mice. In contrast, diabetic wounds led to approximately 55 folds and 24 folds increase in miR-29a and miR-29b1 expression, respectively, compared with intact diabetic skin after 7 days. The circulating macrophages or monocytes originating from the pancreas contain high miR-29ab1 due to the induction of high blood glucose [39]. When the skin is damaged in diabetic mice, the pro-inflammatory phenotype of macrophages induced by damage-associated molecular patterns (DAMPs) secrete abundant IL-1β and TNF-α, which increase the recruitment of circulating and local macrophages and activate them to M1-like phenotype, resulting in an increase of miR-29ab1 [71,72]. Therefore, it can be speculated that the combinatorial stimulation of skin wounds and diabetes showed a cumulative effect on abundant macrophage containing-miR-29a/b1 in the diabetic wound bed. This is consistent with a report by Liu, which showed that reduced expression of miR-192 in quiescent macrophages

could be activated by inflammatory factors [73]. Aberrant miR-29a/b1 elevation is associated with prolonged M1 activation. Reference data showed that miR-29 promoted M1-like remodeling and proinflammation via miR-29 exosomes in a TRAF3-dependent manner, acting as a brake of IL-1β signaling [74]. Hence, an increase in cellular miR-29ab1 levels can inhibit TRAF3 expression, which might initiate upregulation of IL-1β and result in proinflammation, which is consistent with our observations in our miR-29a/b1 deletion mice. In turn, miR-29ab1 stimulates IL-1β and TNF-α expression in cells to aggravate M1 activation [39]. Adverse wound repair occurs in diabetic mice as an autocrine loop of IL-1β/TNF-α/miR-29ab1 stimulation. Consequently, correcting ectopic miR-29a/b1 is favorable for regulating excessive M1 macrophages, which are pivotal for DM-wound repair.

The miR-29 gene family comprises two clusters: miR-29ab1 and miR-29cb2 [75], and the miR-29 family participates in the regulation of gene expression and tissue metabolism, depending on different subtypes and pathological conditions [76,77]. Our previous study demonstrates that the miR-29ab1/SLIT3 axis contributes to regulation of subcutaneous angiogenesis in host immune responses [44]. In this study, we further found the complex functions of miR-29ab1 in the pro-inflammatory response in diabetic wounds and uncovered a novel pharmacological activity of the C@P hydrogel as a suppressor of miR-29ab1 expression. The differences in angiogenesis and collagen production among CS, PUE, and C@P may be attributed to the differential regulation of local macrophage function and miR-29a/b1 levels. Critical evidence shows that the C@P hydrogel may directly benefit diabetic individuals by regulating miR-29ab1 expression of M1 macrophages and inhibition of inflammation. In summary, we found that ectopic high expression of miR-29ab1 is one of the causes of delayed skin wound healing, which can be corrected using the C@P hydrogel. This work may provide insight into the regulation of miRNAs by materials and a new mechanism of wound healing.

5. Conclusions

Diabetic skin wounds are difficult to heal in clinics owing to sustained inflammation. In this study, we found that ectopic high miR-29ab1 was tightly related to inferior diabetic wound healing, which is believed to contribute to prolonged M1 macrophage polarization and elevated TNF-α and IL-1β levels in diabetic mice. Results were verified by the reversed trend observed in miR-29ab1 deletion mice. Chitosan@puerarin hydrogel was synthesized, and results showed that it promotes diabetic wound healing by suppressing ectopic miR-29ab1 mediated macrophages and regulating inflammation. This mechanism may provide a broad spectrum of applications in the material design for diabetic wound healing.

Ethical approval

All animal experiments were approved and carried out with approval from the Shanghai Tongren Hospital Ethics Committee (2021-090-01).

CRediT authorship contribution statement

Xiaoling Zeng: Methodology, Conduct animal experiments, Formal analysis, Visualization, Original manuscript writing, and revision. **Baohui Chen:** Design and synthesis of materials, Physical and chemical characterization of materials, manuscript writing, and revision. **Luping Wang:** Formal analysis. **Yingxiao Sun:** Conduct animal experiments. **Zhao Jin:** Formal analysis. **Xuanyong Liu, Liping Ouyang, Yun Liao:** Conceptualization, Methodology, Project administration, Supervision, Funding acquisition, Resources.

Declaration of competing interest

The authors declare that they have no known competing financial interests or personal relationships that could have appeared to influence the work reported in this paper.

Acknowledgements

This study was supported by grants from the National Natural Science Foundation of China (32071344, 32000938, 81974326, 81403029), Natural Science Foundation of Shanghai (19ZR1449100), Science and Technology Commission of Shanghai Municipality (19JC1415500), and S&T Innovation 2025 Major Special Program of Ningbo (2019B10063).

Appendix A. Supplementary data

Supplementary data to this article can be found online at https://doi.org/10.1016/j.bioactmat.2022.04.032.

References

[1] L.P. da Silva, R.L. Reis, V.M. Correlo, Hydrogel-based strategies to advance therapies for chronic skin wounds, Annu. Rev. Biomed. Eng. 21 (2019) 145–169, https://doi.org/10.1146/annurev-bioeng-060418-052422.
[2] S.A. Eming, P. Martin, M. Tomic-Canic, Wound repair and regeneration: mechanisms, signaling, and translation, Sci. Transl. Med. 6 (2014), 265sr6, https://doi.org/10.1126/scitranslmed.3009337.
[3] X. Yang, R. Yang, M. Chen, KGF-2 and FGF-21 poloxamer 407 hydrogel coordinates inflammation and proliferation homeostasis to enhance wound repair of scalded skin in diabetic rats, BMJ Open Diab. Res. Care 8 (2020), e001009, https://doi.org/10.1136/bmjdrc-2019-001009.
[4] M. Thiersch, M. Rimann, V. Panagiotopoulou, The angiogenic response to PLL-g-PEG-mediated HIF-1α plasmid DNA delivery in healthy and diabetic rats, Biomaterials 34 (2013) 4173–4182, https://doi.org/10.1016/j.biomaterials.2013.02.021.
[5] C.Y. Chen, H. Yin, X. Chen, Ångstrom-scale silver particle-embedded carbomer gel promotes wound healing by inhibiting bacterial colonization and inflammation, Sci. Adv. 6 (2020), https://doi.org/10.1126/sciadv.aba0942 eaba0942.
[6] P. de Oliveira, E.A. Bonfante, E.T.P. Bergamo, Obesity/Metabolic syndrome and diabetes mellitus on peri-implantitis, Trends Endocrinol. Metabol. 31 (2020) 596–610, https://doi.org/10.1016/j.tem.2020.05.005.
[7] M.M. Alvarez, J.C. Liu, G. Trujillo-de Santiago, Delivery strategies to control inflammatory response: modulating M1-M2 polarization in tissue engineering applications, J. Contr. Release 240 (2016) 349–363, https://doi.org/10.1016/j.jconrel.2016.01.026.
[8] K.L. Spiller, R.R. Anfang, K.J. Spiller, The role of macrophage phenotype in vascularization of tissue engineering scaffolds, Biomaterials 35 (2014) 4477–4488, https://doi.org/10.1016/j.biomaterials.2014.02.012.
[9] S. Nassiri, I. Zakeri, M.S. Weingarten, Relative expression of proinflammatory and antiinflammatory genes reveals differences between healing and nonhealing human chronic diabetic foot ulcers, J. Invest. Dermatol. 135 (2015) 1700–1703, https://doi.org/10.1038/jid.2015.30.
[10] W. Zhang, X. Qi, Y. Zhao, Study of injectable Blueberry anthocyanins-loaded hydrogel for promoting full-thickness wound healing, Int. J. Pharm. 586 (2020), 119543, https://doi.org/10.1016/j.ijpharm.2020.119543.
[11] H. Zhao, J. Huang, Y. Li, ROS-scavenging hydrogel to promote healing of bacteria infected diabetic wounds, Biomaterials 258 (2020) 120286, https://doi.org/10.1016/j.biomaterials.2020.120286.
[12] S. Zhang, Y. Liu, X. Zhang, Prostaglandin E(2) hydrogel improves cutaneous wound healing via M2 macrophages polarization, Theranostics 8 (2018) 5348–5361, https://doi.org/10.7150/thno.27385.
[13] J. Wu, A. Chen, Y. Zhou, Novel H(2)S-Releasing hydrogel for wound repair via in situ polarization of M2 macrophages, Biomaterials 222 (2019) 119398, https://doi.org/10.1016/j.biomaterials.2019.119398.
[14] B. Saleh, H.K. Dhaliwal, R. Portillo-Lara, Local immunomodulation using an adhesive hydrogel loaded with miRNA-laden nanoparticles promotes wound healing, Small 15 (2019), 1902232, https://doi.org/10.1002/smll.201902232.
[15] H. Wang, Y. Zheng, Q. Sun, Ginsenosides emerging as both bifunctional drugs and nanocarriers for enhanced antitumor therapies, J. Nanobiotechnol. 19 (2021) 322, https://doi.org/10.1186/s12951-021-01062-5.
[16] S.C. Casey, A. Amedei, K. Aquilano, Cancer prevention and therapy through the modulation of the tumor microenvironment, Semin. Cancer Biol. 35 (Suppl) (2015) S199–s223, https://doi.org/10.1016/j.semcancer.2015.02.007.
[17] L. Zhang, W. Wei, Anti-inflammatory and immunoregulatory effects of paeoniflorin and total glucosides of paeony, Pharmacol. Ther. 207 (2020) 107452, https://doi.org/10.1016/j.pharmthera.2019.107452.
[18] X. Chen, J. Yu, J. Shi, Management of diabetes mellitus with puerarin, a natural isoflavone from Pueraria lobata, Am. J. Chin. Med. 46 (2018) 1771–1789, https://doi.org/10.1142/S0192415X18500891.
[19] X. Chen, L. Wang, S. Fan, Puerarin acts on the skeletal muscle to improve insulin sensitivity in diabetic rats involving μ-opioid receptor, Eur. J. Pharmacol. 818 (2018) 115–123, https://doi.org/10.1016/j.ejphar.2017.10.033.

[20] G.F. Meresman, M. Götte, M.W. Laschke, Plants as source of new therapies for endometriosis: a review of preclinical and clinical studies, Hum. Reprod. Update 27 (2020) 367–392, https://doi.org/10.1093/humupd/dmaa039.
[21] R. Bharti, B.S. Chopra, S. Raut, Pueraria tuberosa: a review on traditional uses, pharmacology, and phytochemistry, Front. Pharmacol. 11 (2020), 582506, https://doi.org/10.3389/fphar.2020.582506.
[22] S. Wang, S. Zhang, S. Wang, A comprehensive review on Pueraria: insights on its chemistry and medicinal value, Biomed. Pharmacother. 131 (2020), 110734, https://doi.org/10.1016/j.biopha.2020.110734.
[23] Q. Ou, S. Zhang, C. Fu, More natural more better: triple natural anti-oxidant puerarin/ferulic acid/polydopamine incorporated hydrogel for wound healing, J. Nanobiotechnol. 19 (2021) 237, https://doi.org/10.1186/s12951-021-00973-7.
[24] C.J. Guo, J.J. Xie, R.H. Hong, Puerarin alleviates streptozotocin (STZ)-induced osteoporosis in rats through suppressing inflammation and apoptosis via HDAC1/HDAC3 signaling, Biomed. Pharmacother. 115 (2019), 108570, https://doi.org/10.1016/j.biopha.2019.01.031.
[25] C.M. Liu, J.Q. Ma, S.S. Liu, Puerarin protects mouse liver against nickel-induced oxidative stress and inflammation associated with the TLR4/p38/CREB pathway, Chem. Biol. Interact. 243 (2016) 29–34, https://doi.org/10.1016/j.cbi.2015.11.017.
[26] H. Xu, M. Hu, M. Liu, Nano-puerarin regulates tumor microenvironment and facilitates chemo- and immunotherapy in murine triple negative breast cancer model, Biomaterials 235 (2020), 119769, https://doi.org/10.1016/j.biomaterials.2020.119769.
[27] J. Yan, Z.Y. Guan, W.F. Zhu, Preparation of puerarin chitosan oral nanoparticles by ionic gelation method and its related kinetics, Pharmaceutics 12 (2020) 216, https://doi.org/10.3390/pharmaceutics12030216.
[28] S. Zhang, Q. Ou, P. Xin, Polydopamine/puerarin nanoparticle-incorporated hybrid hydrogels for enhanced wound healing, Biomater. Sci. 7 (2019) 4230–4236, https://doi.org/10.1039/c9bm00991d.
[29] Z. Yang, R. Huang, B. Zheng, Highly stretchable, adhesive, biocompatible, and antibacterial hydrogel dressings for wound healing, Adv. Sci. 8 (2021), 2003627, https://doi.org/10.1002/advs.202003627.
[30] M. Kharaziha, A. Baidya, N. Annabi, Rational design of immunomodulatory hydrogels for chronic wound healing, Adv Mater 33 (2021), 2100176, https://doi.org/10.1002/adma.202100176.
[31] J. Qu, X. Zhao, Y. Liang, Antibacterial adhesive injectable hydrogels with rapid self-healing, extensibility and compressibility as wound dressing for joints skin wound healing, Biomaterials 183 (2018) 185–199, https://doi.org/10.1016/j.biomaterials.2018.08.044.
[32] Q. Xu, S. A, Y. Gao, A hybrid injectable hydrogel from hyperbranched PEG macromer as a stem cell delivery and retention platform for diabetic wound healing, Acta Biomater. 75 (2018) 63–74, https://doi.org/10.1016/j.actbio.2018.05.039.
[33] Y. Yuan, S. Shen, D. Fan, A physicochemical double cross-linked multifunctional hydrogel for dynamic burn wound healing: shape adaptability, injectable self-healing property and enhanced adhesion, Biomaterials 276 (2021), https://doi.org/10.1016/j.biomaterials.2021.120838, 120838.
[34] S. Wei, P. Xu, Z. Yao, A composite hydrogel with co-delivery of antimicrobial peptides and platelet-rich plasma to enhance healing of infected wounds in diabetes, Acta Biomater. 124 (2021) 205–218, https://doi.org/10.1016/j.actbio.2021.01.046.
[35] W. Zhang, B. Bao, F. Jiang, Promoting oral mucosal wound healing with a hydrogel adhesive based on a phototriggered S-nitrosylation coupling reaction, Adv Mater 33 (2021), 2105667, https://doi.org/10.1002/adma.202105667.
[36] Y. Xu, Y. Li, Q. Chen, Injectable and self-healing chitosan hydrogel based on imine bonds: design and therapeutic applications, Int. J. Mol. Sci. 19 (2018) 2198, https://doi.org/10.3390/ijms19082198.
[37] M. Mu, X. Li, A. Tong, Multi-functional chitosan-based smart hydrogels mediated biomedical application, Expet Opin. Drug Deliv. 16 (2019) 239–250, https://doi.org/10.1080/17425247.2019.1580691.
[38] N. Bhattarai, J. Gunn, M. Zhang, Chitosan-based hydrogels for controlled, localized drug delivery, Adv. Drug Deliv. Rev. 62 (2010) 83–99, https://doi.org/10.1016/j.addr.2009.07.019.
[39] Y. Sun, Y. Zhou, Y. Shi, Expression of miRNA-29 in pancreatic β cells promotes inflammation and diabetes via TRAF3, Cell Rep. 34 (2021), https://doi.org/10.1016/j.celrep.2020.108576, 108576.
[40] S. Wang, B. Chen, L. Ouyang, A novel stimuli-responsive injectable Antibacterial hydrogel to achieve synergetic photothermal/gene-targeted therapy towards uveal melanoma, Adv. Sci. 8 (2021), 2004721, https://doi.org/10.1002/advs.202004721.
[41] C.S. Yee, L. Xie, S. Hatsell, Sclerostin antibody treatment improves fracture outcomes in a Type I diabetic mouse model, Bone 82 (2016) 122–134, https://doi.org/10.1016/j.bone.2015.04.048.
[42] T.P. Fidler, A. Marti, K. Gerth, Glucose metabolism is required for platelet hyperactivation in a murine model of type 1 diabetes, Diabetes 68 (2019) 932–938, https://doi.org/10.2337/db18-0981.
[43] M. Kronlage, M. Dewenter, J. Grosso, O-GlcNAcylation of histone deacetylase 4 protects the diabetic heart from failure, Circulation 140 (2019) 580–594, https://doi.org/10.1161/circulationaha.117.031942.
[44] Y. Liao, L. Ouyang, L. Ci, Pravastatin regulates host foreign-body reaction to polyetheretherketone implants via miR-29ab1-mediated SLIT3 upregulation, Biomaterials 203 (2019) 12–22, https://doi.org/10.1016/j.biomaterials.2019.02.027.
[45] H. Cao, Y. Qiao, F. Meng, Spacing-dependent antimicrobial efficacy of immobilized silver nanoparticles, J. Phys. Chem. Lett. 5 (2014) 743–748, https://doi.org/10.1021/jz5000269.
[46] M.M. Carleton, M.V. Sefton, Injectable and degradable methacrylic acid hydrogel alters macrophage response in skeletal muscle, Biomaterials 223 (2019), 119477, https://doi.org/10.1016/j.biomaterials.2019.119477.
[47] J. Lee, M.P. Rodero, J. Patel, Interleukin-23 regulates interleukin-17 expression in wounds, and its inhibition accelerates diabetic wound healing through the alteration of macrophage polarization, Faseb. J. 32 (2018) 2086–2094, https://doi.org/10.1096/fj.201700773R.
[48] L. Campbell, C.R. Saville, P.J. Murray, Local arginase 1 activity is required for cutaneous wound healing, J. Invest. Dermatol. 133 (2013) 2461–2470, https://doi.org/10.1038/jid.2013.164.
[49] Y. Du, P. Ren, Q. Wang, Cannabinoid 2 receptor attenuates inflammation during skin wound healing by inhibiting M1 macrophages rather than activating M2 macrophages, J. Inflamm. 15 (2018) 25, https://doi.org/10.1186/s12950-018-0201-z.
[50] Y.S. Yi, Roles of ginsenosides in inflammasome activation, J. Ginseng. Res. 43 (2019) 172–178, https://doi.org/10.1016/j.jgr.2017.11.005.
[51] K.M. Smith, M. Guerau-de-Arellano, S. Costinean, miR-29ab1 deficiency identifies a negative feedback loop controlling Th1 bias that is dysregulated in multiple sclerosis, J. Immunol. 189 (2012) 1567–1576, https://doi.org/10.4049/jimmunol.1103171.
[52] M. Hesketh, K.B. Sahin, Z.E. West, Macrophage phenotypes regulate scar formation and chronic wound healing, Int. J. Mol. Sci. 18 (2017) 1545, https://doi.org/10.3390/ijms18071545.
[53] A.R. Saltiel, J.M. Olefsky, Inflammatory mechanisms linking obesity and metabolic disease, J. Clin. Invest. 127 (2017) 1–4, https://doi.org/10.1172/jci92035.
[54] N.X. Landén, D. Li, M. Ståhle, Transition from inflammation to proliferation: a critical step during wound healing, Cell. Mol. Life Sci. 73 (2016) 3861–3885, https://doi.org/10.1007/s00018-016-2268-0.
[55] T.A. Wynn, K.M. Vannella, Macrophages in tissue repair, regeneration, and fibrosis, Immunity 44 (2016) 450–462, https://doi.org/10.1016/j.immuni.2016.02.015.
[56] F. Zhao, B. Lei, X. Li, Promoting in vivo early angiogenesis with sub-micrometer strontium-contained bioactive microspheres through modulating macrophage phenotypes, Biomaterials 178 (2018) 36–47, https://doi.org/10.1016/j.biomaterials.2018.06.004.
[57] Y. Wu, Y. Quan, Y. Liu, Hyperglycaemia inhibits REG3A expression to exacerbate TLR3-mediated skin inflammation in diabetes, Nat. Commun. 7 (2016) 13393, https://doi.org/10.1038/ncomms13393.
[58] K. Garg, N.A. Pullen, C.A. Oskeritzian, Macrophage functional polarization (M1/M2) in response to varying fiber and pore dimensions of electrospun scaffolds, Biomaterials 34 (2013) 4439–4451, https://doi.org/10.1016/j.biomaterials.2013.02.065.
[59] Q. Chen, G.A. Thouas, Metallic implant biomaterials, Mater. Sci. Eng. R Rep. 87 (2015) 1–57, https://doi.org/10.1016/j.mser.2014.10.001.
[60] B. Mi, J. Liu, G. Liu, Icariin promotes wound healing by enhancing the migration and proliferation of keratinocytes via the AKT and ERK signaling pathway, Int. J. Mol. Med. 42 (2018) 831–838, https://doi.org/10.3892/ijmm.2018.3676.
[61] J. Zheng, R. Fan, H. Wu, Directed self-assembly of herbal small molecules into sustained release hydrogels for treating neural inflammation, Nat. Commun. 10 (2019) 1604, https://doi.org/10.1038/s41467-019-09601-3.
[62] X. Liang, Y. Liu, L. Chen, The natural compound puerarin alleviates inflammation and apoptosis in experimental cell and rat preeclampsia models, Int. Immunopharm. 99 (2021) 108001, https://doi.org/10.1016/j.intimp.2021.108001.
[63] M. Qin, J. Jin, Q. Saiding, In situ inflammatory-regulated drug-loaded hydrogels for promoting pelvic floor repair, J. Contr. Release 322 (2020) 375–389, https://doi.org/10.1016/j.jconrel.2020.03.030.
[64] D.X. Xu, X.X. Guo, Z. Zeng, Puerarin improves hepatic glucose and lipid homeostasis in vitro and in vivo by regulating the AMPK pathway, Food Funct. 12 (2021) 2726–2740, https://doi.org/10.1039/d0fo02761h.
[65] H. Bai, N. Kyu-Cheol, Z. Wang, Regulation of inflammatory microenvironment using a self-healing hydrogel loaded with BM-MSCs for advanced wound healing in rat diabetic foot ulcers, J. Tissue Eng. 11 (2020), 2041731420947242, https://doi.org/10.1177/2041731420947242.
[66] Y. Zhao, Z. Li, S. Song, Skin-inspired antibacterial conductive hydrogels for epidermal sensors and diabetic foot wound dressings, Adv. Funct. Mater. 29 (2019), 1901474, https://doi.org/10.1002/adfm.201901474.
[67] L. Zhao, L. Niu, H. Liang, pH and glucose dual-responsive injectable hydrogels with insulin and fibroblasts as bioactive dressings for diabetic wound healing, ACS Appl. Mater. Interfaces 9 (2017) 37563–37574, https://doi.org/10.1021/acsami.7b09395.
[68] E. Roggli, S. Gattesco, A. Pautz, Involvement of the RNA-binding protein ARE/poly (U)-binding factor 1 (AUF1) in the cytotoxic effects of proinflammatory cytokines on pancreatic beta cells, Diabetologia 55 (2012) 1699–1708, https://doi.org/10.1007/s00125-011-2399-7.
[69] V. Bravo-Egana, S. Rosero, R.D. Molano, Quantitative differential expression analysis reveals miR-7 as major islet microRNA, Biochem. Biophys. Res. Commun. 366 (2008) 922–926, https://doi.org/10.1016/j.bbrc.2007.12.052.
[70] L. Ouyang, Y. Sun, D. Lv, miR-29cb2 promotes angiogenesis and osteogenesis by inhibiting HIF-3α in bone, iScience 25 (2022), 103604, https://doi.org/10.1016/j.isci.2021.103604.
[71] S. Kirchner, V. Lei, A.S. MacLeod, The cutaneous wound innate immunological microenvironment, Int. J. Mol. Sci. 21 (2020) 8748, https://doi.org/10.3390/ijms21228748.

[72] K. Van Raemdonck, S. Umar, K. Palasiewicz, TLR7 endogenous ligands remodel glycolytic macrophages and trigger skin-to-joint crosstalk in psoriatic arthritis, Eur. J. Immunol. 51 (2021) 714–720, https://doi.org/10.1002/eji.202048690.
[73] X.L. Liu, Q. Pan, H.X. Cao, Lipotoxic hepatocyte-derived exosomal MicroRNA 192-5p activates macrophages through rictor/akt/forkhead box transcription factor O1 signaling in nonalcoholic fatty liver disease, Hepatology 72 (2020) 454–469, https://doi.org/10.1002/hep.31050.
[74] L.T. Le, T.E. Swingler, N. Crowe, The microRNA-29 family in cartilage homeostasis and osteoarthritis, J. Mol. Med. (Berl.) 94 (2016) 583–596, https://doi.org/10.1007/s00109-015-1374-z.
[75] A.J. Kriegel, Y. Liu, Y. Fang, The miR-29 family: genomics, cell biology, and relevance to renal and cardiovascular injury, Physiol. Genom. 44 (2012) 237–244, https://doi.org/10.1152/physiolgenomics.00141.2011.
[76] E. Hiroki, J. Akahira, F. Suzuki, Changes in microRNA expression levels correlate with clinicopathological features and prognoses in endometrial serous adenocarcinomas, Cancer Sci. 101 (2010) 241–249, https://doi.org/10.1111/j.1349-7006.2009.01385.x.
[77] M.E. Widlansky, D.M. Jensen, J. Wang, miR-29 contributes to normal endothelial function and can restore it in cardiometabolic disorders, EMBO Mol. Med. 10 (2018), e8046, https://doi.org/10.15252/emmm.201708046.